A probabilistic radar forward model for small ice particles

Robert S. Schrom[1] and Matthew R. Kumjian[1]

[1]*The Pennsylvania State University, 503 Walker Building, 16802 State College, United States*

(Dated: 22 June 2018)

Introduction

A radar forward model connects physical properties of hydrometeors to radar measurements. These forward simulators are important for microphysical model validation and interpreting radar observations. The wide variety of shapes and sizes of ice particles, as well as their importance in precipitation growth, make it difficult to fully understand ice microphysical processes. By evaluating microphysical models with radar measurements, we may be able to make progress in better understanding these processes. The growth of branched planar crystals is particularly important in the development of precipitation in the mid-latitudes (Andrić et al., 2013; Kumjian and Lombardo, 2017) and within mixed-phase Arctic clouds (e.g., Oue et al., 2016)

Forward simulations of the radar variables are performed first by calculating the radar scattering properties of the individual simulated ice particles. Because the bulk radar signal contains samples of numerous hydrometeors within a given volume of the atmosphere, we calculate it using the integrated radar scattering properties of ice particles over probability distributions of their size, orientation, and shape. With exception to the orientation distribution, the distribution quantities are predicted by microphysical models and are input into the forward model. Thus, errors from the forward model are separate from the errors in the microphysical model; the errors and uncertainty in the forward model are the focus of this study.

Because of the errors in simplified representations of branched planar crystals in scattering models (e.g., Schrom and Kumjian, 2018), we need to incorporate detailed-shape scattering calculations into forward models to accurately simulate the polarimetric variables. Given the natural variability in ice crystal shape, we also use these detailed-shape calculations to provide estimates of the uncertainty in the radar scattering properties due to shape ambiguity. We then apply this forward model to microphysical model output with a simplified Monte Carlo method to evaluate the uncertainty in forward model simulations of the polarimetric radar variables.

Scattering calculations

Branched planar crystals have both six-fold symmetry along their characteristic a-axis dimensional plane and reflectional symmetry across their c-axis. Therefore, we introduce a method to generate realistic structures in the "top-view" plane of ice crystals, and use these shapes in the scattering calculations for a forward model. In an effort to generate 2-D branched planar crystal structures that 1) are able to produce a high degree of variability and 2) depend on a limited number of clearly defined physical quantities, we have developed a procedure for generating these 2-D shapes. These physical quantities are illustrated in 1. The similarities between all of the structures we generate with this procedure are that they all have a solid ice core with a given size, six main branches that grow off of the core, evenly spaced subbranches of fixed width that grow off of the main branches, and interiors bounded by a star-shaped outline.

Single-particle radar scattering properties

We use the discrete dipole approximation (DDA) code of Yurkin and Hoekstra (2011) to perform detailed scattering calculations for branched planar crystals. Because the DDA code requires a set of point dipole locations, we use the quantities defined above to generate 2-D polygons for each branched planar crystal and then fill these polygons with a 2-D dipole lattice. We then create the 3-D shape by extending the 2-D structure of dipoles into 3-D along the crystal c-axis.

Both simplified results from ice crystal growth theory (e.g., Sheridan et al., 2009) and observational studies (e.g., Auer and Veal, 1970) suggest that the aspect ratio ($\phi = \frac{c}{a}$, where c is the c-axis length and a is the a-axis length) for branched planar crystals evolves approximately according to a power law during vapor depositional growth. To capture the natural evolution of branched planar crystals, we use a range of power law exponent coefficients to relate the aspect ratio to the size. We assume that all crystals start as hexagonal plates with $\phi = 1$ and a-axis length $a_{min} = 1\mu$m allowing us to use the following relation for the power law:

$$\phi = \left(\frac{a_{min}}{a}\right)^b, \tag{2.1}$$

where b is the power law exponent and the units of a are microns.

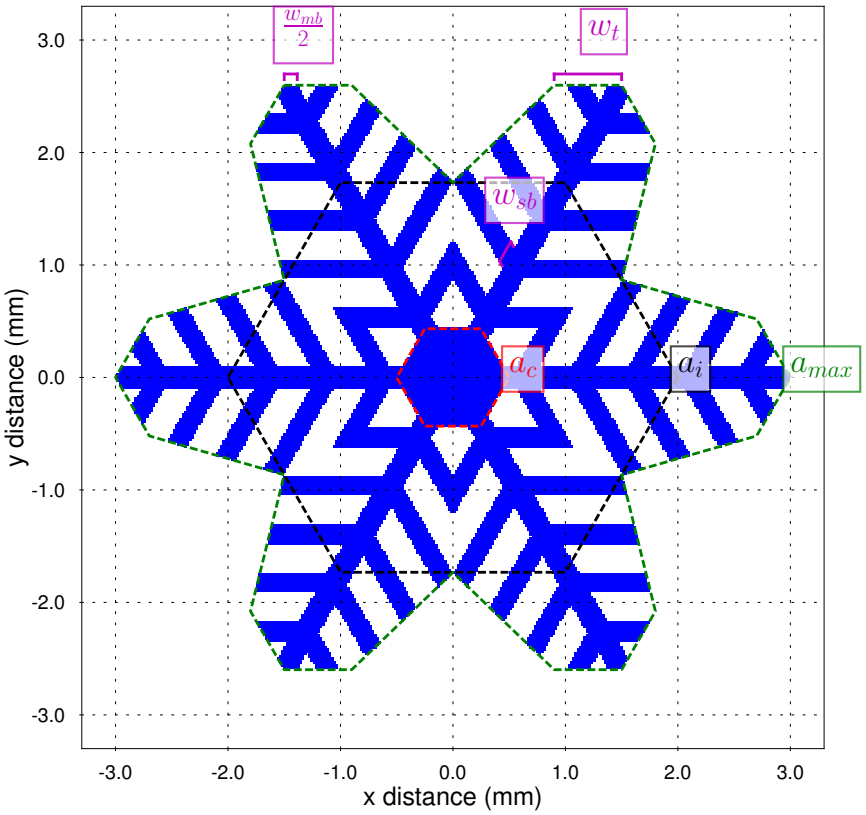

Figure 1: Plot of dipole locations for a branched planar crystal with outlines of the a_c, a_i, and star-shaped regions ploted in dashed red, black, and green lines, respectively. The particular values of w_t, w_{mb} and w_{sb} are labeled and plotted in magenta. The number of subbranches n_{sb} in this example is 5.

Table 1 shows the ranges of each quantity used to generate the 3-D branched planar crystal shapes. The ranges of values of the structure quantities are chosen to generally span the limited observations of effective density (e.g., Jensen et al., 2015). We also set a_{max} to 3 mm and create subsets of the ice particle shapes at 12 a-axis lengths ranging from 0.01 mm to 3 mm and spaced in equal increments according to the square root of their values.

Table 1: Description of the ranges of values (inclusive) used to generate the branched planar crystal shapes and sizes we use for the scattering calculations presented herein. The following values are fixed for all of the ice crystals: number of dipoles along the c axis $n_z = 9$ and $a_{max} = 3$ mm. These ranges of quantities results in a total of 10368 DDA calculations.

Quantity	description	minimum value	maximum value	number of values	spacing
a	crystal a-axis side length	0.01 mm	3.0 mm	12	square-root linear
b	aspect ratio-size power law coefficient	0.40	0.65	6	linear
f_b	subbranch fractional area coverage	0.2	0.9	4	linear
f_i	inscribed hexagon fractional distance	0.1	0.9	3	linear
f_t	tip width fraction	0.3	0.9	2	linear
a_c	core a-axis side length	0.1 mm	0.5 mm	3	linear
n_{sb}	number of subbranches per main branch	2	4 mm	2	linear

Equivalent solid-ice spheroids

For branched planar ice crystals that are small relative to the radar wavelength, we can assume that two pieces of independent information sufficiently describe their backscatter. Therefore, we may represent the detailed-shape scattering by equivalent solid-ice spheroids, where the independent information is contained in the solid-ice spheroid maximum dimension and thickness. These solid-ice spheroids are equivalent in the sense that they have the same backscattering properties as those from detailed-shape calculations (e.g., using DDA). Given our interest in the bulk radar reflectivity factor at horizontal polarization (Z_H) and Z_{DR}, we use σ_h and Z_{DR} from the DDA calculations to constrain the backscatter-equivalent d and h. Therefore, for a given branched planar crystals with σ_h and Z_{DR} calculated from DDA, the equivalent solid-ice spheroid will have the same

σ_h and Z_{DR}.

Given that we focus on small-particle scattering, we perform DDA calculations at S band (with $\lambda = 100$ mm) for branched planar crystals generated using the method described above and the properties listed in Table 1. We then determine the equivalent spheroids from the DDA-calculated σ_h and Z_{DR} for each crystal. Using formulas for the scattering of homogeneous spheroids in the Rayleigh regime from Ryzhkov et al. (2011), we are then able to iteratively determine the maximum dimension and thickness that correspond to the same σ_h and Z_{DR} as those from DDA, using a fixed number of iterations for each particle that results in errors $< 1\%$.

From the equivalent spheroid dimensions and the corresponding maximum dimensions and thicknesses of the branched planar crystals, we calculate the percentage changes in maximum dimension P_d and thickness P_t with:

$$P_d = 100 \times \frac{d_{eqv} - d}{d} \tag{2.2}$$

$$P_h = 100 \times \frac{h_{eqv} - h}{h}, \tag{2.3}$$

where d_{eqv} and h_{eqv} are the maximum dimension and thickness, respectively of the equivalent solid-ice spheroid. In order to simplify the process of mapping bulk physical properties to scattering properties, we can exploit the fact that small-particle scattering is a smooth function of the particle size by performing polynomial fits of P_d and P_h for the branched planar crystals as functions of effective density and aspect ratio; the maximum dimension is then incorporated into the mapping function by determining the dimensions of the equivalent spheroids from (2.2) and (2.3).

To test the accuracy of this mapping procedure, we compare the σ_h and Z_{DR} from the DDA calculations to the σ_h and Z_{DR} from the polynomial fits based on the maximum dimension, aspect ratio, and effective density of the branched planar crystals used in the DDA calculations. The comparison for Z_{DR} is shown in Fig. 2, where the highest counts of particles are found near the one-to-one line. We also find similar results for the comparison of σ_h (not shown).

Forward model evaluation

Estimation of forward model uncertainty

To calculate the bulk radar variables and estimate their uncertainties, we use distributions of aspect ratio, effective density, and number concentration (e.g., from microphysical model output) to first calculate the percentage dimensional changes for particles within each model bin using the polynomials fit to the scattering calculations. We then add random Gaussian noise (corresponding to the single-particle scattering variability) to the percentage dimensional changes calculated for each particle. Using the maximum dimension and thickness simulated by the model and the perturbed dimensional changes, we then calculate the equivalent spheroid dimensions. To calculate the radar scattering properties for each of these equivalent spheroids, we use the formulas for homogeneous spheroids in Ryzhkov et al. (2011) at a given wavelength, and then calculate σ_h, σ_v, and Z_{DR} for the individual ice crystals.

Once we have these bulk radar variables for a given realization of Gaussian noise, we then repeat this process for N_{sam} realizations, randomly sampling percentage dimensional changes for each ice crystal size to calculate N_{sam} bulk radar variables. From these samples of the forward-simulated bulk radar variables, we may then get estimates of their uncertainty solely due to uncertainty in the precise shape of branched planar crystals.

Arctic mixed-phase cloud simulations

To provide an example of the forward model described herein, we examine a case of vapor depositional growth described in Oue et al. (2016). During this case, a cloud was present within the lowest 2 km of the atmosphere; temperatures in this region ranged from between -20 °C to -10 °C. Surface observations taken during the early portion of the case indicated branched planar crystals were the predominant ice crystal habit (see Fig. 3c of Oue et al., 2016).

Radar observations during this case from the Atmospheric Radiation Measurement (ARM) X-band scanning precipitation radar (XSAPR) at Barrow, Alaska show relatively high Z_{DR} throughout the cloud, with low Z_H generally increasing towards the ground (Fig. 3). These radar observations indicate either plate or branched planar crystals growing by vapor deposition and sedimenting. This general microphysical evolution is supported by the sounding that indicates supersaturated conditions throughout the lowest 1-1.5 km of the atmosphere, along with favorable temperatures for vapor depositional growth. In

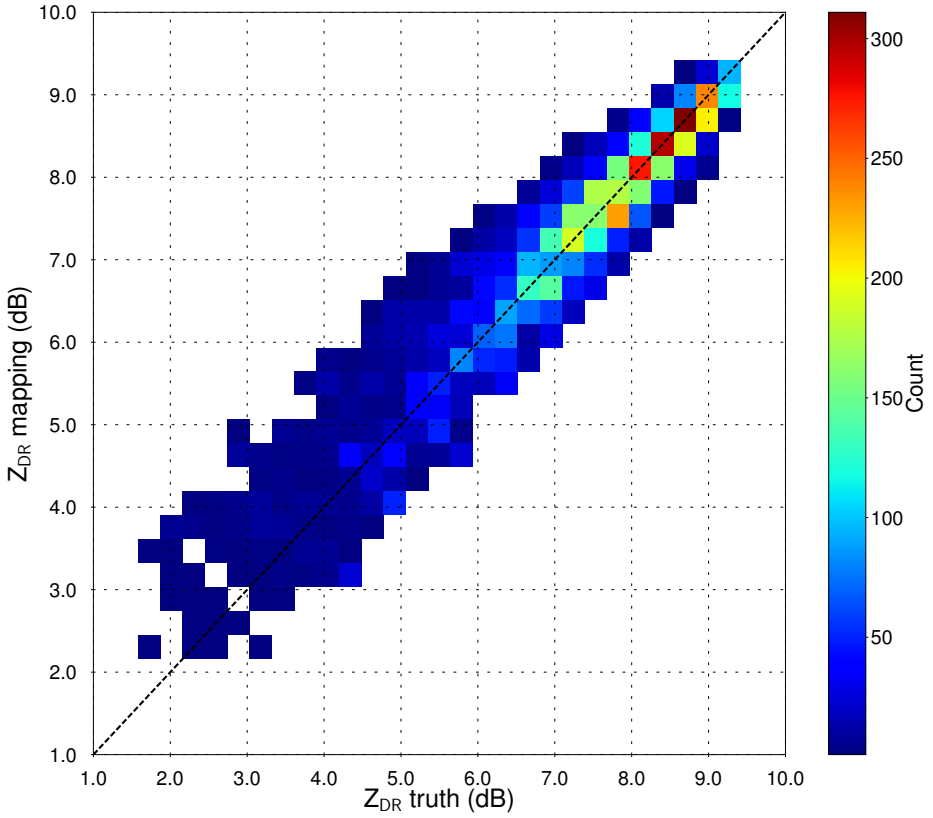

Figure 2: Comparison of Z_{DR} calculated with DDA and using the equivalent-scattering-spheroid mapping procedure for the branched planar crystals defined in Table 1. Pairs of calculations for each branched planar crystal are plotted as counts within given bins of Z_{DR} from DDA (x axis) and from the corresponding Z_{DR} values from the mapping procedure (y axis). The one-to-one line is indicated by the black dashed line.

addition, relatively low liquid water paths through the cloud system at the time of these radar observations suggests that riming was a limited factor in the growth of the ice particles (e.g., Fig. 3b of Oue et al., 2016).

In order to simulate this case, we use an idealized 2-D kinematic model coupled to a bin microphysical model with adaptive habit microphysics that allows for the natural evolution of maximum dimension, aspect ratio, and effective density. This model is similar to that implemented by Harrington et al. (2014) but for explicit prediction of the ice particle properties within each bin. The kinematic framework of this model means that the flow is fixed in time, with one set of idealized updraft and downdraft cells. Both the flow field and the growth/sublimation of ice change the temperature and humidity of the environment. The simulations start with the 2-D domain initialized with the same environment from the sounding and run for 1 hour. After this time, we take profiles of the ice particle size, aspect ratio, and effective density spectral distributions within the updraft and use these profiles to calculate the radar variables. From the uncertainty estimation in our forward model, we derive the standard deviation at each height level in the model profile.

The results for the simulated Arctic mixed-phase cloud case are shown in Fig. 3. Simulations of Z_H show similar shape between the reduced-density spheroid and equivalent-solid ice spheroid calculations, with the equivalent spheroids resulting in a slightly larger Z_H at all heights. The $\pm\sigma$ interval from the forward model ranges from 1 dB to 3 dB, with the largest uncertainty near the highest Z_H, around 700 m above ground level (AGL).

A much larger difference between the reduced-density spheroid calculations and the forward model is present in the simulated Z_{DR} profiles. The shapes of the simulated Z_{DR} profiles show notable differences; the Z_{DR} calculated with the reduced-density spheroids has maximum value at the top of the profiles, decreasing by about 1 dB to the minimum value of 3.7 dB at 700 m height. In contrast, Z_{DR} from the equivalent-spheroid forward model is 1.5-2.5 dB higher and decreases gradually by around 0.5 dB from the top of the profile to around 300 m AGL. The uncertainty in Z_{DR} from the forward model shows a maximum $\pm\sigma$ interval of 0.6 dB around 750 m AGL, where the model-simulated density of branched planar crystals is modestly reduced.

The observations are generally consistent with the simulations; Z_H has a similar shape between 0.9-1.4 km AGL, with

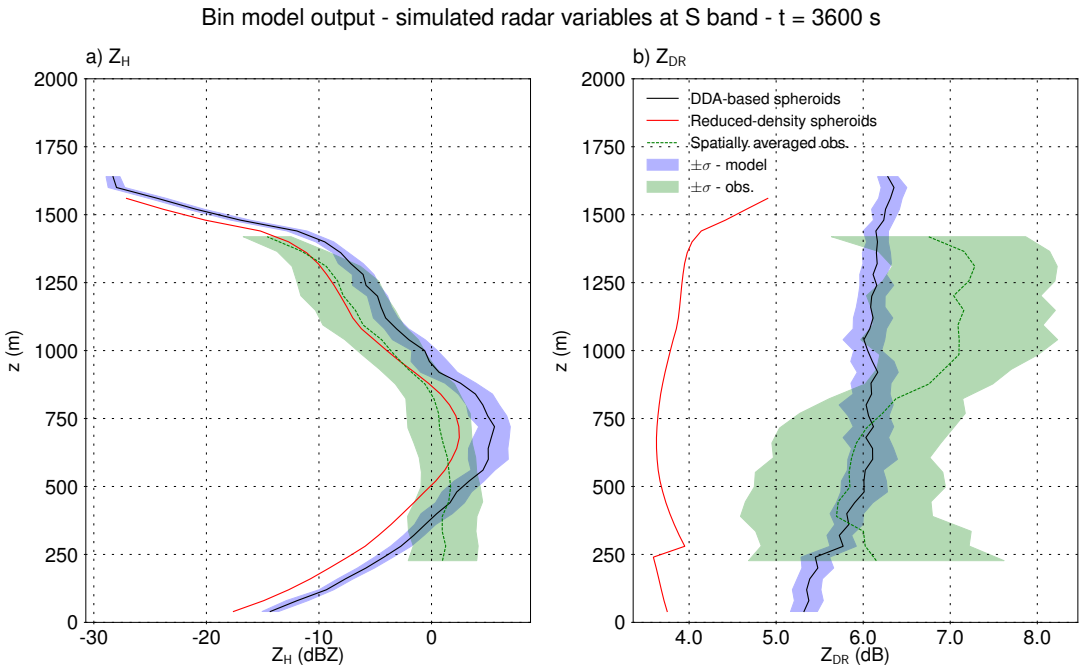

Figure 3: Simulated profiles of a) Z_H and b) Z_{DR} at S band for the model-simulated ice crystals within a profile through the updraft of the simulated cloud. The red lines indicate the simulations of the radar variables using homogeneous, reduced-density spheroids in the Rayleigh approximation, the black lines indicate the mean radar profiles simulated using the forward model described herein, and the blue shading indicates the one-standard-deviation interval of simulated radar variables at each height. Observed profiles of the mean Z_H and Z_{DR} (averaged horizontally from an RHI taken through the cloud) are plotted in green dashed lines. The green shaded regions about the means indicates the one-standard-deviation interval based on the spatial variabilities of the profiles over the averaging region.

values remaining relatively constant below 0.9 km. The spatial variability of Z_H is also larger than that due to the scattering variability from the forward model. The mean observed Z_H happens to be closer to the simulated Z_H from the reduced-density model. However, this correspondence is not particularly meaningful, given the large uncertainties in ice nucleation rates and updraft speeds used in the model. Additionally, the Z_{DR} observations (relatively independent of ice number concentration) show much better correspondence to the equivalent-scattering spheroid forward model simulations. The spatial variability in the observed Z_{DR} is much larger than the scattering uncertainty in the forward model, suggesting that faithfully capturing ice nucleation and microscale dynamic features of Arctic cloud systems are potentially more important than errors that may arise from assuming a particular branched planar crystal. However, using homogeneous, reduced-density spheroids in the scattering model may still produce biases in Z_{DR} that dominate even the processes that govern the spatial variability of the radar observations.

Conclusions

Polarimetric radar measurements of branched planar crystals have the potential to improve our understanding of the growth of these particles within mixed-phase cloud systems. To aid in this goal, we present a forward model that accurately maps bulk ice-crystal physical properties to their microwave scattering properties. Natural variability in the precise ice particle structure that is unspecified by a microphysical model allows us to additionally estimate the uncertainty in forward simulations of the radar variables.

When applied to bin microphysical model output for an Arctic mixed-phase cloud case, we see generally better comparisons to the observed Z_{DR} for the equivalent-spheroid forward model than for the homogeneous, reduced-density spheroid calculations. The spatial variability of the observed Z_H and Z_{DR} is larger than the scattering uncertainty from the forward model. This high spatial variability suggests that accurately comparing radar observations to those simulated from model output requires consideration of the variability in ice growth environments that can be reasonably simulated by the model. If the model provides much coarser or more idealized representations of the precipitation evolution, careful spatial and or temporal averaging of both the observations and model is required.

Acknowledgement

The work contained in this extended abstract is based on a paper in preparation for submission to the Journal of Applied Meteorology and Climatology. Funding for the authors comes from DOE grant No. DE-SC0013953. We thank Jerry Harrington for providing the code for the microphysical model and Hans Verlinde, Eugene Clothiaux, and Kultegin Aydin for their helpful discussions on this work.

References

J. Andrić, M. R. Kumjian, D. S. Zrnić, J. M. Straka, and V. M. Melnikov, "Polarimetric signatures above the melting layer in winter storms: An observational and modeling study," *J. Appl. Meteor. Climatol.*, vol. 52, pp. 682–700, 2013.

A. H. Auer and D. L. Veal, "The dimension of ice crystals in natural clouds," *J. Atmos. Sci.*, vol. 27, pp. 919–926, 1970.

J. Y. Harrington, K. Sulia, and H. Morrison, "A method for adaptive habit prediction in bulk microphysical models. Part I: Theoretical development," *J. Atmos. Sci.*, vol. 70, pp. 349–364, 2014.

M. P. Jensen, W. A. Petersen, A. Bansemer, N. Bharadwaj, L. D. Carey, D. J. Cecil, S. M. Collis, A. D. D. Genio, B. Dolan, J. Gerlach, S. E. Giangrande, A. Heymsfield, G. Heymsfield, P. Kollias, T. J. Lang, S. W. Nesbitt, A. Neumann, M. Poellot, S. A. Rutledge, M. Schwaller, A. Tokay, C. R. Williams, D. B. Wolff, S. Xie, and E. J. Zipser, "The midlatitude continental convective clouds experiment (MC3E)," *Bull. Amer. Meteor. Soc.*, 2015, in press.

M. R. Kumjian and K. A. Lombardo, "Insights into the evolving microphysical and kinematic structure of northeastern U.S. winter storms from dual-polarization Doppler radar," *Mon. Wea. Rev.*, vol. 145, pp. 1033–1061, 2017.

M. Oue, M. Galletti, J. Verlinde, A. Ryzhkov, and Y. Lu, "Use of X-band differential reflectivity measurements to study shallow Arctic mixed-phase clouds," *J. Appl. Meteor. Climatol.*, vol. 55, pp. 403–424, 2016.

A. V. Ryzhkov, M. Pinsky, A. Pokrovsky, and A. Khain, "Polarimetric radar observation operator for a cloud model with spectral microphysics," *J. Appl. Meteor. Climatol.*, vol. 50, pp. 873–894, 2011.

R. S. Schrom and M. R. Kumjian, "Bulk-density representations of branched planar ice crystals: Errors in the polarimetric radar variables," *J. Appl. Meteor. Climatol.*, vol. 57, pp. 333–346, 2018.

L. M. Sheridan, J. Y. Harrington, D. Lamb, and K. Sulia, "Influence of ice crystal aspect ratio on the evolution of ice size spectral during vapor depositional growth," *J. Atmos. Sci.*, vol. 66, pp. 3732–3743, 2009.

M. A. Yurkin and A. G. Hoekstra, "The discrete-dipole-approximation code ADDA: Capabilities and known limitations," *J. Quant. Spectrosc. Radiat. Transfer*, vol. 112, pp. 2234–2247, 2011.